Research Square

Preprints are preliminary reports that have not undergone peer review.
They should not be considered conclusive, used to inform clinical practice,
or referenced by the media as validated information.

Solar Driven Agricultural Greenhouse Integrated with Desalination System; Energy-Water-Food Nexus

Kabir Abdullahi (kabir.abdullahi@ejust.edu.eg)
Egypt-Japan University of Science and Technology https://orcid.org/0000-0003-2315-1568
Alaa Salah
City of Scientific Research and Technological Applications
Hassan Fath
Egypt-Japan University of Science and Technology

Research Article

Keywords: Sustainable greenhouse, Desalination, Condenser, Solar distillers, Natural ventilation

Posted Date: May 22nd, 2020

DOI: https://doi.org/10.21203/rs.3.rs-23546/v1

License: This work is licensed under a Creative Commons Attribution 4.0 International License.
Read Full License

Solar Driven Agricultural Greenhouse Integrated with Desalination System: Energy-Water-Food Nexus

Kabir Abdullahi[1, 2]*, Alaa H. Salah[3] and Hassan Fath[1]

[1]Department of Environmental Engineering, Egypt-Japan University of Science and Technology, Alexandria 21934, Egypt

[2]Abuja Environmental Protection Board, Cadastral Zone 776, Central Business District, Abuja Nigeria

[3]Computer Based Engineering Applications Department, Informatics Research Institute, City of Scientific Research and Technological Application, New Borg El Arab City, 21934 Alexandria, Egypt

* Correspondence: kabir.abdullahi@ejust.edu.eg

Abstract

This study presents the effective performance of a sustainable solar driven agricultural greenhouse (GH) self-reliant of energy and irrigation water via desalination. The GH is furnished with infrastructures such as; (i) - an inlet condenser for cool air exchanger and partial water production, (ii) - an internal cavity for crop production (iii) - roof transparent solar distillers (TSD) for solar desalination and partial shading and (iv)- a thermal chimney for natural air ventilation. A mathematical model is developed to predict the performance of the sustainable GH system. A coupled approach of MATLAB/Simulink and computational fluid dynamics (CFD) based on three simulation models were used: solar radiation, thermal energy balance and CFD model. Two parametric studies were carried out. The first one analyzed the effects of different air velocity on the system thermal performance and natural ventilation rate. The second study assessed the effects of different covering material on the transmitted solar radiation. Results from the model shows that 8.5 MJ/m^2.day of total solar radiation is transmitted into the GH. The greenhouse air temperature is lowered by 5°C and humidified by 20%, to satisfy the required conditions necessary for plant growth. Maximum water yield of 11.5 L/m^2.day was obtained, aided by the addition of Al-metal

net. Additionally, 2.6 kWh/m^2.day of power is consumed by the air-cooling condenser. At air velocity of 0.3 m/s, there is a natural tendency of air to flow by draft, due to air temperature difference of up to 4 °C. Furthermore, glass and EVA cover materials transmit 52 and 48 % of solar radiation into the GH respectively. The proposed system will enable the parallel production of water and food and enhance economical plant productivity.

Keywords: Sustainable greenhouse; Desalination; Condenser; Solar distillers; Natural ventilation

1. Introduction

Solar driven agricultural greenhouse integrated with desalination system represent one of the best applied example of the energy-water-food nexus. This integrated system not only provide its own irrigation water, it also provide a controlled environment necessary for food production and has the potential to generate electrical energy via photovoltaic (PV) cells [1]. The UN world water development report 2015 states that by 2050, an increase in 55 % of global water demand will be observed, and the world's agricultural sector will be required to generate 60 % more food, reaching up to 100 % in the developing nations [2]. The 2017 World Health Organization (WHO) reports that, with the prevailing climate change situation, more than 50 % of the world population will exist in high water stress areas by 2030 [3]. The intensifying water crisis is also associated to food production since agriculture accounts for 70 % of all freshwater usages [4], hence fresh water supply is one of the most significant future issues [5]. The evident increasing demand for food, energy and water, coupled with the ever-increasing scarcity of land resources, this study aims to tackle these issues by proposing the investment of solar energy into desalination and greenhouse systems.

An agricultural greenhouse (GH) is an enclosed transparent house used to protect

55 crops from critical ambient climate conditions and pests, and provide the opportunity
56 to adjust the indoor microclimate suitable for crop growth and production, both in terms
57 of quantity and quality [6]. GH enables year-round crop production and improves the
58 yield and quality of crops through control of the physical environmental factors such as
59 light, water, temperature, relative humidity, CO2 concentration, and ventilation [7]. GH
60 technology can guarantee the sustainable and secure food production by increasing the
61 production yield up to ten times more [1], and decreasing the 11.8 m^3/d per capita water
62 requirements by 80 % compared to conventional cultivation [2, 3]. However, GH
63 energy consumption can be up to one hundred times more [8]. Thus, one of the
64 substantial technical challenges of GHs is management of energy consumption [9].
65 Renewable energy technologies provide access to the secure and environmentally
66 sustainable supply of energy and can be cost-effective as well [10]. For sustainability,
67 solar thermal appears to be the most sustainable energy resource [11]. Since the GH
68 itself functions as a solar collector, solar energy utilization can lead to a reduction in
69 production cost [12].

70 All GH systems, irrespective of physiographical location, consist of essential
71 climate control mechanisms and components, and depending on their design and

72 complexity, they are capable of providing a major or minor amount of environmental
73 control, and consequent plant growth and productivity. The major fundamental GH
74 microclimate environment is strongly reliant on available solar radiation, temperature
75 manipulation, humidity control, CO_2 concentration and air ventilation [13, 14].
76 Temperature management is essential to influencing plant growth and development,
77 with an average range of 17°C to 27°C, over which there is a near linear positive
78 response in terms of increased growth [15]. Humidity (RH) in GHs is controlled to
79 ensure adequate transpiration and also reduces fungal infection. As a general guide, it
80 is often recommended that GH RH be maintained within the range 60-90 % suitable for
81 healthy plant growth. CO_2 enrichment is also vital in GH production with most plants
82 showing a positive response to increased CO_2 levels up to 1,000 - 1,500 ppm [13, 15].
83 Ventilation is necessary during summer periods to prevent excess rise of GH
84 temperature above the ambient air. The rate of ventilation varies between 20 and 180
85 air changes per hour [3].

86 Agricultural GHs have shown great complexity and diversity depending on its
87 location across the globe. For cold climates, GH are specifically designed to provide a
88 warmer environment for crops to grow, such as the so-called active (or heated)

89 greenhouses equipped with several heating devices. Meanwhile, GH combined with
90 shading, ventilation (passive GH), or cooling systems are used in hot climates to control
91 the inner environment. Ghani et al. [16] comprehensively reviewed several GH designs
92 features in hot and arid climates. The review involved GH shape, dimensions,
93 orientation, cooling methods, and the renewable technologies applicable in GHs. Due
94 to the continuous increase in energy prices and climate concerns, the energy
95 consumption in GH systems became one of the main challenges especially in hot
96 climate [17]. In general, two methods can be used to reduce the energy consumption of
97 agricultural GH systems. These methods are the integration of semi-transparent
98 photovoltaic (PV) and solar distillation units on the GH roof [18, 19]. Several integrated
99 GH systems utilizing solar radiation above plant needs have been documented. Yano et
100 al. [20] established two prototypes of semi-transparent- photovoltaic (PV) modules
101 proposed for GH roof applications. The yearly electrical energy production estimate
102 showed that these PV modules are potentially suitable for GHs in high solar radiation
103 regions, where electrical energy production could be high. Yohannes and Fath, [21]
104 developed an agriculture GH model with in-built Transparent Photo-Voltaic (TPV)
105 panels to be energy self-sufficient and produce irrigating water for the hot

106 environmental conditions of Abu Dhabi, UAE. Hassan et al. [19] investigate the effect
107 of cooling system condenser properties on the interior climatic conditions inside a GH
108 integrated with on-roof TPV. The results demonstrate that the GH satisfy the required
109 micro-climatic conditions for plants growth and be self-sufficient of irrigating water
110 during a hot day for Abu Dhabi, UAE.

111 Many studies are concerned with the integration of a solar distillers with a GH
112 system. Fath and Abdelrahman [22] studied the numerical performance of a GH
113 covered with on-roof transparent solar still at 30° inclination. The GH shows to
114 withstand harsher environmental conditions when integrated with an on-roof solar still.
115 Radhwan [23] developed a stepped-solar-still for GH heating and humidification. The
116 total daily yield of the solar stills is about 4.92 L/m^2, and the daily average efficiency
117 is about 63%. Chaibi [24] performed a numerical and experimental deviation study of
118 a small water desalination module to be placed on a GH roof, and obtained a 25%
119 deviation between calculated and measured water production. Mari et al. [25] conduct
120 an experimental and theoretical study to examine the performance of 28 on-roof solar
121 still integrated into a GH. Results revealed approximately 52% reduction in solar
122 radiation inside the GH, the theoretical model also overestimate the water yield by

123 approximately 15% higher than the measured one. Radhwan and Fath [26]
124 experimentally investigate the thermal performance of an agricultural GH consisting of
125 24 on-roof solar stills distillation system. For the summer condition of Jedda, Saudi
126 Arabia, the results showed that the temperatures inside the GH are 8–10° (at GH inlet)
127 and 3–6° (at GH outlet) below ambient temperature. The relative humidity inside the
128 GH is found to vary between 20% and 35% above ambient conditions, satisfying the
129 comfort zone of the plant growth. They obtained a relatively small water production
130 range from 1.7 to 2.5 L/d, mainly due to relatively high glass temperature. A solar GH
131 with built-in water desalination system and humidification-dehumidification (HDH)
132 system was analytically studied [27]. This integrated system uses the excess solar
133 radiation (excess of the crop requirement) to desalinate water and reduce the cooling
134 load of the greenhouse. The results showed that, by controlling the fresh-air ratio and
135 condenser by-pass ratio, the interior climate of the GH will satisfy the comfort zone for
136 plant growth. The system can produce about 8.6 kg/m^2.day of water. Rabhy et al. [28]
137 developed an experimental and numerical analyses of a transparent solar distiller
138 suitable for agricultural GH. The system results show about 37.5% of irrigation water
139 can be produced, whiles the power consumption of the GH cooling system can be

140 reduced by 60%. Other developed integrated system include the 'Watergy' GH system,
141 developed for integrated water treatment, solar thermal energy collection and advanced
142 food production suitable in the arid and Mediterranean regions [29]. De Zwart [30] also
143 developed a system called 'Sunergy', which is a semi-closed GH that is closed during
144 periods with high solar radiation, to enable harvesting of solar energy at moderately
145 high temperatures, and allows ambient air exchange during cloudy days and at night,
146 for dehumidification. Seawater GH is another strategy developed based on solar
147 distillation units for arid countries in the Middle East to challenge the high temperature,
148 water salinity, and water scarcity problems. These concepts were examined using both
149 experimental setups [31] and energy and mass balance models [32]. The main
150 conclusions of this studies were that semi-transparent solar still modules can be
151 integrated into a GH roof in order to control the solar radiation and produce fresh water,
152 which could meet the irrigation demand of GHs.

153 The main contribution of this study is to integrate all the elements of energy-water-
154 food nexus into a system capable of producing food, water and reducing energy
155 consumption, while also cutting costs and improving the quality of the combined
156 services. A sustainable GH system is developed, which was integrated with transparent

157 solar distillers (TSD) and equipped with a chilled water condenser at the entry of the
158 GH cavity. The design concepts are based on micro-climate control strategies,
159 renewable energy water production sources and application of innovative covering
160 materials. Firstly, it presents and uses a method to couple MATLAB/Simulink with
161 computational fluid dynamics (CFD) for GH climate modelling. The MATLAB model
162 were used to predict surface temperatures, condenser effects, water production and
163 power consumption, which were then used as boundary condition in the CFD model to
164 determine the micro-climatic condition of the GH cavity. Secondly, the effects of
165 different operating parameters on the micro-climatic conditions inside the GH (air
166 temperature and relative humidity), water production and electrical power consumption
167 of the GH are investigated. The simulations are carried out to evaluate the performance
168 of the GH for the metrological conditions of a Mediterranean climate. Furthermore, the
169 GH model was analyzed for its natural ventilation performance. This developed model
170 will provide the basis for further investigation and designing next generation GHs, for
171 sustainable agriculture in the MENA-GCC and other water-stressed regions.

172 **2. Materials and methods**

173 *2.1 System Description*

The conceptual configuration of the GH is demonstrated in Fig. 1. Briefly, the GH system consist of an interior glass covered plant cavity, a chilled water condenser at the entry of the GH cavity, a vertical and inclined riser, set of transparent solar distillers placed on the risers, a thermal chimney and a vertical down comer channel. The GH structure was designed facing the south in order to receive maximum solar radiation whiles minimizing heat loss. Geometrical dimension of the GH is giving in Table 1.

Ventilation fresh air (a1) at ambient condition enters the GH through an inlet condenser. In the condenser, the air is partially cooled and humidified, depending on the ambient temperature and relative humidity. The cool air (a2) then mixes with the bypassing air and moves through the interior GH cavity (ai), where it gains heat and water vapor through convection and plant transpiration. The heated air then leaves the GH cavity through an outlet condenser (a3), where it gets cooled to saturation condition and condense the water derived from plants transpiration. The cool air (a4) then mixes with the bypassing air and flow through the vertical (a5) and inclined risers (a6), to gain extra heat from solar stills and glass covers. Depending on the seasonal condition, the heated air then either leaves the GH to the atmosphere through a thermal chimney or partially recirculated from the down comer (a7) into the GH cavity to mix with the fresh

ambient air. In the current paper, the outlet condenser is not active (switched off) and no air recirculation through the down comer.

The integrated transparent solar distiller is illustrated in Fig. 2. The solar distillers are oriented to face the south with a cover tilt angle of 30°, which is equal to the solar latitude angle of the target study area [28]. The solar distillers are designed to be transparent to enable solar light reach plant region for photosynthetic process. Further, the solar distillers will serve as partial shading thereby reducing the GH cooling load and utilize the excess solar radiation (above plant need) for water desalination. The solar still desalination works based on evaporation and condensation [2]. Solar radiation passes through the glass cover and converts the saline water into vapor. The water vapor flows up and condenses on the inner surface of the inclined cover due to temperature differences. The purely desalinated water is then collected via the distillation trough [33]. Due to the low gained output ratio (GOR) of solar still desalinations, an aluminum (Al) metal net is added to the base of the distillers to enhance productivity by increasing the absorption of solar radiation. A parametric study is performed to determine the effect of net area ratio on the total solar radiation transmitted into the GH cavity.

2.2 Model Development

208 In this sustainable GH analysis, an integrated approach of MATLAB/Simulink and
209 ANSYS-CFD models are used in three steps of calculations. The process is summarized
210 as follows; Firstly, a transient mathematical model was used to calculate the
211 instantaneously incident global solar radiation received by the GH covers based on a
212 Clear Day Solar Flux Model [27, 34]. Secondly, a transient thermal model based on
213 energy and mass balance equations were used for each component of the GH system to
214 predict the thermal behavior of the system. The equations were solved using MATLAB.
215 Finally, a 2-D ANSYS-CFD model was then developed to determine the microclimatic
216 condition (in terms of air velocity, temperature, relative humidity and water vapor)
217 within the GH cavity.

218 Fig. 3 shows briefly the system methodology. The calculated solar radiation by the
219 clear sky model and the ambient conditions (of temperature, RH, wind speed) were
220 used as inputs for the thermal model. The glass surface temperatures and condenser air
221 temperature predicted by the thermal model were used as input for the boundary
222 condition of the CFD model. The continuity, energy, species and mass transport
223 equations were solved numerically. The CFD model methodology will be explained in
224 Section 2.2.3.

2.2.1 Solar Radiation Model

The instantaneous overall solar radiation incidental on the inclined surface of the GH depends on the declination & solar altitude angle, latitude and surface inclination angle. In this model, the instantaneous global solar radiation incident on each GH surface is predicted according to Eqns. 1-6 [27, 34].

$$I_{\beta} = I_{B\beta} + I_{D\beta} + I_{R\beta} \quad (1)$$

$$I_{B\beta} = Ae^{-k*sec\theta_z} * cos\theta_z \quad (2)$$

$$I_{D\beta} = C * Ae^{-k*sec\theta_z} * 0.5(1 - cos\beta) \quad (3)$$

Where I_{β} is the incident global solar radiation, $I_{B\beta}$ is the direct beam radiation. $I_{D\beta}$ is the diffused radiation. $I_{R\beta}$ is the reflected solar radiation.

The zenith angle ($\boldsymbol{\theta_z}$) on an inclined surface of the GH is calculated according to Eqn.4,

$$cos\theta_z = sin\delta sin\emptyset + cos\delta cos\emptyset cos\omega \quad (4)$$

Declination angle ($\boldsymbol{\delta}$) is calculated as below,

$$\delta = 23.45sin\left(360\frac{284+n}{365}\right) \quad (5)$$

To calculate the total solar radiation received on the GH and TSS components, the Eqn. below is used,

241 $$s_t = \sum A_i I_i \quad (6)$$

242 Where $\boldsymbol{A_i}$ and $\boldsymbol{I_i}$ represent the area and the total incident radiation reaching the ith

243 section. The values of A, k and C are 1069 W/m^2, 0.205 and 0.134 respectively for

244 21st June giving from the ASHRAE model [35]. Solar radiation inside the GH is

245 calculated based on the above equations using the transmissivity of each cover material

246 layer and water.

247 *2.2.2 Thermal Model*

248 To predict the transient surface temperature of the GH cover components, heat air

249 exchange, condensed water from moist air condenser, yield produced from the TSS and

250 the electrical power consumed by the condenser are achieved from the equations of

251 energy and mass balance. The mathematical model is developed with the following

252 assumptions [36]:

253 (1) Clear sky solar radiation model is applied

254 (2) Air is assumed transparent for long and short-wave radiation and its absorptivity is

255 neglected

256 (3) Plant thermal properties are equivalent to that of water due to the high content of

257 water in the plant

(4) Relative humidity and temperature of circulating air are presumed to be uniform

(5) GH component temperatures are lumped (i.e. same throughout)

(6) Temperature of earth below the ground is assumed constant at 15 °C and evaporation of the floor is negligible.

(7) GH is assumed to be properly insulated with no leakage through the walls.

(8) Thermal analysis is based on quasi-steady state conditions inside the greenhouse due to transient behavior for short time intervals and heat transfer is one-dimensional.

The main governing equations are listed below, Eqns. 7-11, [19, 27]

For transient temperature change for each GH and TSD components;

$$\frac{dT}{dt} = \frac{1}{M.C_p}(\sum Q_{in} - \sum Q_{out}) \tag{7}$$

For air flow, Eqn 8 applies;

$$\dot{m_a}(h_o - h_{in}) = (\sum Q_{in} - \sum Q_{out}) \tag{8}$$

For condensed water from the condenser;

$$\dot{m_c} = \dot{m_{cond}}(w_{in} - w_{out}) \tag{9}$$

From the TSD, the produced distillate is calculated as follows;

$$\dot{m_{TSD}} = \frac{Q_e}{h_{fg}} \tag{10}$$

The electrical power is calculated as follows;

$$power = \frac{\dot{m_{cond}}(h_{in} - h_{out})}{COP} \quad (11)$$

The input data for the thermal model are the calculated solar radiation and the climate metrological data of temperature, relative humidity and wind speed. Fig. S1 (supplementary material) illustrates the universal energy and water vapor fluxes within the GH, which were used to define the mass balance and energy balance equations of the proposed model. Fig. S2 (supplementary material) illustrates the flow chart of the mathematical model procedure.

2.2.3 CFD Model

2.2.3.1 Governing Equations

To study the internal climatic condition of the GH cavity, heat transfer processes are solved using the CFD code (ANSYS Fluent). The flow inside the GH was considered as two-dimensional, an-isothermal, fully turbulent and incompressible flow. The CFD code uses the finite volume method for solving the governing equation of fluid flow and heat transfer based on mass, energy and momentum conservation, i.e. the Navier–Stokes equation. The transport equation of air flow based on the Navier–Stokes equation is given by [37];

$$\frac{\partial \rho \psi}{\partial t} + \nabla \cdot (\rho \vec{v} \psi) = \nabla\big(\Gamma \nabla \psi\big) + S_m \quad (12)$$

Where ρ, t, ψ and ∇ are the density, time, concentration variable and divergence operator respectively. $\vec{v}$ and Γ are the velocity vector and diffusion coefficient. The source term, S_m is added due to crop transpiration.

The Energy Equation balance is giving by equation 13 [22];

$$\frac{\partial}{\partial x_i}[u_i(\rho e + p)] = \frac{\partial}{\partial x_i}\left[\left(K + \frac{C_p \mu_t}{Pr_t}\right)\frac{\partial T}{\partial x_i} - \sum_j h_j J_j\right] + S_h \quad (13)$$

Where e, K and h_j represent the total fluid energy, thermal conductivity and and species sensible enthalphy respectively.

The species transport equation and conservation equation for air and water vapor fraction was activated using the mass fraction of H2O (w/w) described by equation 14 [38].

$$\frac{\partial}{\partial t}\left(\rho Y_{H_2O}\vec{v}\right) = \frac{\partial}{\partial t}\left[(\rho D_{H_2O} + \frac{\mu_t}{Sc_t})\frac{\partial Y_{H_2O}}{\partial t}\right] + S_{H_2O} \quad (14)$$

Where S_{H_2O} represent water vapor added or removed from the air due to condensation or evaporation. The constant D_{H_2O} is the diffusion coefficient of water vapor into air which is equal to 2.88x 10^{-5}; Sc_t is the turbulent Schmidt number which is equal to 0.7.

To account for turbulences, the standard k– ε model with wall function was used [39]. This model solves for turbulent kinetic (k) and the rate of dissipation of energy (ε) in

unit volume and time. This model has been used in GH CFD simulations with success, providing good agreement with experimental results [40]. The equations for k and ε are giving below, respectively.

$$\frac{\partial}{\partial t}(\rho k) + \frac{\partial}{\partial x_i}(\rho k u_i) = \frac{\partial}{\partial x_j}\left[\left(\mu + \frac{\mu_t}{\sigma_k}\right)\frac{\partial k}{\partial x_j}\right] + G_k + G_b - \rho\varepsilon - Y_M + S_k \quad (15)$$

$$\frac{\partial}{\partial t}(\rho \varepsilon) + \frac{\partial}{\partial x_i}(\rho \varepsilon u_i) = \frac{\partial}{\partial x_j}\left[\left(\mu + \frac{\mu_t}{\sigma_\varepsilon}\right)\frac{\partial \varepsilon}{\partial x_j}\right] + C_{1\varepsilon}\frac{\varepsilon}{k}(G_k + C_{3\varepsilon}G_b) - C_{2\varepsilon}\rho\frac{\varepsilon^2}{k} + S_\varepsilon \quad (16)$$

From the equations, G_k and G_b represent the generated turbulence kinetic energy due to mean velocity gradients and buoyancy respectively, Y_M represents the dilation fluctuation contribution in compressible turbulences. The constants are giving below [22].

$$C_{1\varepsilon} = 1.44, C_{2\varepsilon} = 1.92, C_\mu = 0.09, \sigma_k = 1.0, \sigma_\varepsilon = 1.3$$

The plant was considered as porous media with the source term governed by the Darcy–Forchheimer equation which include the viscous loss term and inertial resistance loss term [41].

The Darcy law is giving by;

$$S_i = -\left(\frac{\mu}{\alpha}u + C_2\frac{1}{2}\rho|u|u\right) \quad (17)$$

Where α and C_2 represent the permeability and inertial resistance factors of the porous medium, whose values are chosen to represent the crop under consideration.

2.2.3.2 Geometry creation and grid generation

The 2D computational domain was created using ANSYS Design Modeler 18.2. The geometrical characteristics of the GH were assigned according to what is presented in Table 1. A 2D structured mesh was generated using Ansys Mesh workbench, which consist of approximately 71,000 cells. A structured Cartesian mesh was chosen to limit the numerical diffusion of errors and facilitate calculation convergence.

Four different element sizes of the structural grids are used to test the grid independence; including the coarse (0.5 m), medium (0.3 m), fine (0.1 m) and very fine (0.05 m). Two of the simulation parameters, air velocity out (V_{out}) and pressure in (P_{in}), are selected to evaluate the effect of the grid density. The V_{out} and P_{in} calculated from the coarse and medium grid deviate significantly, while the fine and very fine grid represent similar results. Therefore, the fine grid system was used to conduct our simulations, considering the efficiency and computing accuracy. The quality of the grid was checked by applying the skewness parameter. The skewness parameter indicates how ideal a cell shape is. The mesh used gave a maximum skewness parameter of 0.5, which falls into the "good" range, according to the Ansys Fluent manual [42].

2.2.3.3 Method of solutions and boundary conditions

Academic ANSYS FLUENT V18.2 was used to carry out the CFD analysis. The

344 computational domain was meshed using a two-dimensional structured mesh with
345 71,748 cells. The CFD code solves the transport equation using the finite volume
346 method for each cell. To account for pressure velocity coupling, the SIMPLE algorithm
347 was used [41]. The CFD numerical model parameters are enumerated in Table 2. The
348 convergence criterion is set to 10^{-6} for the continuity, momentum and turbulence
349 equations, and 10^{-8} for the energy equation.

350 The glass cover and air temperature variations, which were predicted by the thermal
351 model, were considered as the boundary conditions for the CFD model. The interior
352 GH cavity were simulated in the CFD model for full day, in an hourly quasi-steady-
353 state condition. The main working fluid in this simulation is a mixed species of water
354 vapor and air, whose density depends on the operating pressure while the specific heat,
355 thermal conductivity and viscosity were taken as a function of temperature. The plant
356 region is simulated as porous material with viscous resistance $\boldsymbol{\alpha^{-1}}$ = 2.532 m^{-2}, inertial
357 resistance $\boldsymbol{C_2}$ = 1.6 m^{-1} and porosity of 40%. The participating solid material in the
358 porous media calculation is considered as a fully developed tomato plant whose
359 properties are detailed in Table 3. Thermo-physical properties of other materials like
360 glass, water and ground are giving in Table 4 [43, 44].

361 *2.2.4 Parametric study*

362 The general performance of the GH system on four different air velocities (0.6, 0.5,
363 0.4, 0.3 m/s) were examined. Four different cover materials were also studied; (a) glass,
364 (b) Ethylene vinyl acetate film (EVA), (c) polyethylene (P.E), (d) polyvinyl chloride
365 film (PVC), whose optical properties are given in Table 5 [43, 45].

366 **3. Results and discussion**

367 *3.1 Model Validation*

368 To validate this model, the interior GH temperature and relative humidity is firstly
369 compared between simulation and published data of [27] for the ambient condition of
370 21st June. Fig. 4 shows the simulation and validation data of the average air temperature
371 and relative humidity inside the GH cavity. The trend of the air temperature (Fig. 4a)
372 shows close agreement especially during solar hours, the difference between the
373 simulation and validation values was always less than 1°C. Regarding the relative
374 humidity (Fig. 4b), the agreement was particularly good during the solar hours, the
375 maximum difference between both values occurred after midnight, when the validation
376 values dropped more quickly than those predicted by the CFD model. In all cases, the
377 maximum relative humidity difference was less than 7 %. A good comparison between

the two values suggest that the simulation of temperature and relative humidity propagation inside the GH interior is successful. Therefore, in view of the validation results of the model, the CFD model proved to be a satisfactory predictive model that could be used to predict the temperature and airflow distributions in GHs. Hence, the CFD can therefore, be a very useful tool in the study of the internal microclimatic conditions of the GH system.

3.2 Effect of TSD on transmitted solar radiation

The key for designing transparent GHs is to get enough solar radiation into the GH. The threshold of solar intensity required for plants photosynthetic process is 8.5 MJ/m^2.day [46, 47]. During the summer, excess solar radiation about twice the plant need is available. To utilize the excess solar intensity, this study integrates transparent solar distillers into GH roof. To improve productivity of the distillers, an Al-metal net were added to the base of the solar distillers to increase solar absorptivity and decreases transmissivity into the GH. Fig. 5 shows the effect of the Al-metal net on the transmitted solar radiation and the daily variation of the direct solar radiation reaching the GH. Firstly, we study the effect of the Al-metal net area ratio to the solar still base. In Fig. 5a, when the net area ratio is zero (i.e. no metal net added), 14 MJ/m^2.day of total solar

radiation is available during the day. By increasing the net-area ratio, the total solar radiation transmitted into the GH decreases, reaching the required threshold of 8.5 MJ/m^2.day at a net area ratio of 0.75. Fig. 5b present hourly variation of the transmitted solar radiation into the GH through each cover, for the maximum radiation day of 21st June, with glass cover material. The solar intensity varied in a sinusoidal way with total available direct solar radiation of 8.5 MJ/m^2.day, the maximum value of 250 W/m^2 recorded during solar hours. The solar distillers reduce the transmitted solar radiation by ~50%. These solar intensity data were then used to compute the temperature on individual roof and wall of the GH using the standard ASHRAE model.

3.3 GH system operational performance

The operational performance of the GH in terms of air temperature, relative humidity, freshwater production and power consumption of the air-cooling condenser are analyzed. The evolution of these factors throughout the day for the examined air velocity are presented.

Fig.6 illustrate the hourly variation of the average air temperature in the GH cavity for the 21st of June, for the four examined air velocity and the ambient temperature. In all cases, the GH air temperature is lower than the ambient temperature because of the

412 effect of condenser air-cooling, and the solar distillers serving as a partial shading.
413 While the ambient air temperature varies between 24°C to 31°C, the GH (cavity)
414 average air temperature varied from 20°C to 26°C. During this day, as the sun rose
415 around 6:00 AM, GH temperature began to rise until it reached 26°C. As the sun set,
416 around 6:00 PM, the solar radiation intensity and ambient temperature dropped, the GH
417 air temperature also dropped accordingly to a value below 22°C. Despite the change in
418 air velocity, the GH air temperature were similar, satisfying the required condition
419 needed for plant growth.

420 In Fig. 7, the average air relative humidity inside the GH cavity and the ambient
421 for the four examined air velocities are giving. The GH air relative humidity is 15 to
422 20% higher than that of the ambient. This is because the air gets humidified in the
423 condenser and from plant transpiration. The ambient relative humidity varies between
424 45% and 80%, in the GH it varies between 60% and 90%. The relative humidity obeys
425 the sinusoidal trend with its minimum value at midday. Favorably, lower relative
426 humidity at mid-day aid the air-cooling condenser in reducing the high ambient air
427 temperature. The difference of the average air relative humidity among the examined
428 air velocities are not important, since the mechanism of vapor transfer remains the same.

In all cases, the air relative humidity inside the GH cavity is within the satisfactory values (comfort zone) for plants growth.

Fig. 8 present the hourly accumulated water production from the TSD and the condenser for the examined air flow rates. The addition of Al-metal net enhances the productivity of the TSD, producing averagely over 60% of the accumulated water. The major difference in water production from the examined air velocities is found in the condenser distillate, since the condensed water production depends on the mass flow rate of air passing through the condenser. At air flow rate of 0.3 m/s, over 9 L/m^2.day of water is produced. The distillate water production increases with an increase in air flow velocity, an additional 2.5 L/m^2.day of water production was observed at increasing air flow velocity from 0.3 to 0.6 m/s. Overall, the GH system is capable of producing freshwater which exceed the average irrigation water demand of a GH (2 L/m^2.day) [28, 48],

Fig. 9 shows the accumulated power consumed by the air-cooling condenser for the examined air flow rates. At air flow rate of 0.3 m/s, 1.3 kWh/m^2.day of energy is consumed by the air-cooling condenser to produce 2.7 L/m^2.day of fresh water. Increasing the air flow rate from 0.3 m/s increases the energy consumption by 0.43

446 kWh/m^2.day for each step increase. This is due to the increase in mass flow rate of air
447 passing through the condenser. At 0.6 m/s, the energy consumption is about 2.6
448 kWh/m^2.day, producing 5.4 L/m^2.day of fresh water. Integrating an agricultural GH
449 with transparent solar distillers decreases power consumption for air cooling by
450 approximately 60% [28]. For all examined air flow rates, the condenser consumed
451 reasonable amount of energy for air cooling and distillate production, these results are
452 consistent with Hassan et al. [19]

453 *3.4 Optimal growing conditions*

454 An appropriate microclimate for plant growth and development is characterized by
455 the solar light availability, when it is up to 8.5 MJ/m^2.day, the temperature range
456 varying between 14 and 28 °C, RH of 60 – 90% and air velocity between 0.2 to 0.5 m/s.
457 In order to assess the efficiency of each examined air flow rate, distributions and
458 profiles for air velocity, temperature and humidity for the mid-day at a flow rate of 0.5
459 m/s are presented. Fig. 10 shows the CFD simulation results for GH air temperature,
460 velocity vectors and relative humidity contours at 12 P.M of 21st June with glass cover
461 material. At this time, the ambient air temperature is 304 K, the outside relative
462 humidity is 46 % and the wind speed is 0.5 m/s.

Fig. 10a indicates the temperature distribution inside the GH cavity. The GH air temperature in the plant region is slightly cooler than the ambient air, with an average GH air temperature of 299 K. This is due to the cooling effect created by the inlet condenser. The CFD model also shows the solar distiller region (roof) of the GH as the hottest surface, which intercept majority of the solar radiation. The GH air temperature is uniform for most of the GH cross section, with the left region of the cross section slightly warmer. This is due to the air heating by convection and plant transpiration as it passes through the GH cavity, and transferring the heat to the GH roof, which becomes warmer than other regions in the GH.

Fig. 10(b) and (c) show the relative humidity and water mass fraction contours predicted by the CFD model at 12 P.M for the same set of boundary conditions. Fig. 10b shows an increase in humidity immediately after the condenser, since the air gets humidified in the condenser unit. As the air flows in the plant region, the air becomes warmer and humidified from plant transpiration. The average air relative humidity in the plant region is 62 %, which is higher than the ambient RH of 45%. The water mass fraction (Fig. 10c) also increases in a stream wise direction in the plant zone, due to water vapor generated inside the plant region. The water mass fraction was slightly

higher in areas with higher air temperatures (Fig. 10a), since hot air holds more water vapor.

Fig. 10d illustrate the air velocity vectors developed inside the GH at 12 P.M for the 21st June. The air velocity depends on the opening area, which is 1 m^2, with an average air velocity of 0.5 m/s at the inlet opening. In the plant region, the air velocity is damped due to high resistance of plant to air flow. This causes a strong stream of air to flow over the plant, while a weaker stream flow under the plant (as seen from the stream function contours). The average air velocity in the plant region varies between 0.1- 0.2 m/s, which perfectly suits plant growth conditions.

3.5 Natural ventilation performance

This sustainable GH will aim to rely on natural ventilation driven by two mechanisms, namely the wind induced pressure field around the GH and the buoyancy force induced by the warmer and more humid air in the GH riser. Natural ventilation is effective if the outside temperature is low compared to GH riser air temperature, where the difference in density between the inside and outside air causes natural draft [49]. Air temperature and humidity differences between the inside and outside of a GH produce forces that drive flow. The natural tendency for hot and humid air to rise and

accumulate towards the upper part of a space leads to stable stratification, and this has a significant influence on the flow patterns within the GH. The determining factor in the form of the vertical stratification is the location of the openings. The warm and humid air will flow out over the upper area of the opening and the cool air will enter through the lower area of the opening.

Buoyancy driven ventilation is significant only at low wind speeds. At low wind speed, the buoyancy effect is the main driving force of ventilation in a GH with plant. To evaluate the natural ventilation of this GH, the temperature field on the inclined riser generated by the four different air velocities is shown in Fig.11. During the day, the air temperature at the inclined riser (T_a6) is higher than the ambient air temperature at wind speed of 0.3 and 0.4 m/s. At speed of 0.3 m/s, the air temperature at the inclined riser is 4 °C higher than the ambient. This is due to the absorbed solar radiations by the solar stills and dissipated subsequently as latent and sensible heat inside the GH. During the non-solar hours, the outside air is warmer than the inside GH due to the cooling effect created by the condenser. To achieve natural ventilation at night, the condenser may have to be turned OFF. Hence, natural ventilation could be maintained in the GH especially during the daytime. This conditions also satisfy the air exchange rate of 0.7

514 AC/min.

515 *3.6 Covering material parametric study*

516 GH sustainability depends largely on cover material, as it influences the GH
517 microclimate and protect plants from adverse weather conditions. The evolution of
518 basic factors such as transmitted solar radiation, interior air temperature and water
519 production for each examined cover material are presented. Fig. 12a present the
520 instantaneous total solar radiation transmitted into the GH cavity for the examined
521 cover materials for the maximum radiation day of 21st June. The highest transmitted
522 solar radiation is achieved with the glass and EVA cover, with 52 and 48 % solar
523 radiation transmitted into the GH respectively. The PVC cover allows lower
524 transmittance (~ 30 %) due to its high absorptivity, which may become less in winter
525 season. The air temperature and relative humidity differences inside the GH cavity for
526 the studied cover materials are not significant (data not shown), because the main
527 mechanism of heat transfer is from convection of the entering air stream and the effect
528 of air-cooling condenser. For water production, Fig. 12b shows the accumulated water
529 production for the examined cover materials. Less water is expected to be produced
530 from the transparent solar distillers for PVC and P.E covers due to high material

absorptivity and low transmitted solar radiation. Although sufficient amount of fresh water is expected to be produce from the air-cooling condenser unit.

4 Conclusions

In this study, a newly developed solar driven agricultural greenhouse for air cooling, and solar energy application for irrigation water production is presented. The potentials of using an integrated TSD-GH system was investigated, combining water production and agricultural farming in the same area. The potential harmony between solar radiation availability and the demand for irrigation water is illustrated. A new coupled approach of MATLAB/Simulink and CFD modelling methodology was developed to predict the performance of the sustainable GH system. This approach takes advantage of the strength of each tool to study, with accuracy, the full functionality and requirement needed to operate a sustainable GH integrated with solar desalination system. The calculations are implemented for the external environmental condition of 21st June, representing the maximum radiation day of Borg-El-Arab, Egypt.

In general, the excess solar radiation was utilized, allowing 8.5 MJ/m^2.day of solar intensity threshold for plant photosynthetic process. An AL-metal net was added to trap the excess solar radiation for enhanced desalination water production. A parametric

548 study was carried out to investigate the effect of different air flow velocity and covering
549 materials. Increasing the air velocity by 0.1 m/s increases the water production by 0.75
550 L/m^2.day, and power consumption by 0.43 kWh/m^2.day. At wind speed of 0.3 m/s, air
551 temperature at the inclined riser is 4 °C higher than the ambient condition. At this
552 condition, there is a tendency of the air to flow by natural draft, hence reducing the fan
553 power. At air velocity of 0.5 m/s (base line), the average air temperature and relative
554 humidity in the GH cavity were 26 °C and 62 % respectively, at 12:00 of the maximum
555 radiation day. For different covering materials, the highest transmitted solar radiation
556 is achieved with glass and EVA cover, with 52 and 48 % solar radiation transmitted into
557 the GH respectively.

558 In general, to overcome the MENA-GCC drought, this GH is designed to reach a
559 water autonomous irrigation situation by investigating the potential of providing
560 conventional and nonconventional water sources for a water efficient GH. This self-
561 sustainable GH will allow sufficient cooling to enable crop production in the extreme
562 summer climate of the Mediterranean regions. The proposed system will also allow
563 parallel production of food and water and enhance plant productivity. The desalination
564 components may perhaps enable regional progress in GH production into arid and

MENA-GCC regions. In the next step of this research, a comprehensive economic analysis and development of an experimental model are proposed. The economic analysis will include the capital and operating cost of the integrated system. The major capital cost will include building construction, cooling system, transparent solar distillers, irrigation system, water storage tank, fan ventilation systems, lightening and other machinery and equipment. Operational cost will consist of labor cost, material input, marketing, fertilizer and repair and maintenance cost. The experimental validation will be built along the shores of the Mediterranean Sea in Borg Al-Arab Egypt, using cost effective and sustainable materials.

Declarations

Availability of data and materials

All data generated or analyzed during this study are available from the corresponding author on reasonable request.

Competing interests

The authors have declared no conflict of interests.

Funding

This work was supported by Egypt-Japan University of Science and Technology.

582 **Authors' contributions**

583 All authors read and approved the final manuscript.

584 **Acknowledgements**

585 The first author acknowledges Egyptian Ministry of Higher Education (MoHE) and
586 Japan International Cooperation Agency (JICA) for providing all the needed facilities
587 to conduct this research.

588 **References**

589 1. H. Esmaeli and R. Roshandel, “Optimal design for solar greenhouses based on
590 climate conditions,” Renew. Energy, vol. 145, pp. 1255–1265, 2020.
591 2. N. Shekarchi and F. Shahnia, “A comprehensive review of solar-driven desalination
592 technologies for off-grid greenhouses,” Int. J. Energy Res., vol. 43, no. 4, pp. 1357–
593 1386, 2019.
594 3. A. Entezari, R. Z. Wang, S. Zhao, E. Mahdinia, J. Y. Wang, Y. D. Tu, and D. F.
595 Huang, “Sustainable agriculture for water-stressed regions by air-water-energy
596 management,” Energy, vol. 181, pp. 1121–1128, 2019.
597 4. J. Farfan, A. Lohrmann, and C. Breyer, “Integration of greenhouse agriculture to
598 the energy infrastructure as an alimentary solution,” Renew. Sustain. Energy Rev.,

599 vol. 110, no. August 2018, pp. 368–377, 2019.

600 5. T. Sakamoto, T. Ogawa, H. Nada, K. Nakatsuji, M. Mitani, B. Soberats, K. Kawata,
601 M. Yoshio, H. Tomioka, T. Sasaki, M. Kimura, M. Henmi, and T. Kato,
602 “Development of Nanostructured Water Treatment Membranes Based on
603 Thermotropic Liquid Crystals: Molecular Design of Sub-Nanoporous Materials,”
604 Adv. Sci., vol. 5, no. 1, Jan. 2018.

605 6. J. I. Montero, E. J. Van Henten, J. E. Son, and N. Castilla, “Greenhouse
606 engineering: New technologies and approaches,” Acta Hortic., vol. 893, pp. 51–64,
607 2011.

608 7. G. Giacomelli, N. Castilla, E. Van Henten, D. Mears, and S. Sase, “Innovation in
609 greenhouse engineering,” Acta Hortic., vol. 801 PART 1, no. July 2015, pp. 75–88,
610 2008.

611 8. G. L. Barbosa, F. D. Almeida Gadelha, N. Kublik, A. Proctor, L. Reichelm, E.
612 Weissinger, G. M. Wohlleb, and R. U. Halden, “Comparison of land, water, and
613 energy requirements of lettuce grown using hydroponic vs. Conventional
614 agricultural methods,” Int. J. Environ. Res. Public Health, vol. 12, no. 6, pp. 6879–
615 6891, Jun. 2015.

9. R. H. E. Hassanien, M. Li, and W. Dong Lin, “Advanced applications of solar energy in agricultural greenhouses,” Renewable and Sustainable Energy Reviews, vol. 54. Elsevier Ltd, pp. 989–1001, Feb-2016.

10. IRENA 2015 "Renewable Energy in the Water, Energy & Food Nexus"

11. J. J. Cartelle Barros, M. Lara Coira, M. P. de la Cruz López, and A. del Caño Gochi, “Assessing the global sustainability of different electricity generation systems,” Energy, vol. 89, pp. 473–489, Sep. 2015.

12. G. K. Ntinas, V. P. Fragos, and C. Nikita-Martzopoulou, “Thermal analysis of a hybrid solar energy saving system inside a greenhouse,” Energy Convers. Manag., vol. 81, pp. 428–439, 2014.

13. A. M. Syed and C. Hachem, “Review of Design Trends in Lighting, Environmental Controls, Carbon Dioxide Supplementation, Passive Design, and Renewable Energy Systems for Agricultural Greenhouses,” J. Biosyst. Eng., vol. 23, no. 1, pp. 28–36, 2019.

14. A. Yano, A. Furue, M. Kadowaki, T. Tanaka, E. Hiraki, M. Miyamoto, F. Ishizu, and S. Noda, “Electrical energy generated by photovoltaic modules mounted inside the roof of a north–south oriented greenhouse,” Biosyst. Eng., vol. 103, no. 2, pp.

633 228–238, Jun. 2009.

634 15. A. Al-Ibrahim, N. Al-Abbadi, and I. Al-Helal, “PV greenhouse system - System
635 description, performance and lesson learned,” Acta Hortic., vol. 710, pp. 251–264,
636 2006.

637 16. S. Ghani, F. Bakochristou, E. M. A. A. ElBialy, S. M. A. Gamaledin, M. M.
638 Rashwan, A. M. Abdelhalim, and S. M. Ismail, “Design challenges of agricultural
639 greenhouses in hot and arid environments – A review,” Engineering in Agriculture,
640 Environment and Food, vol. 12, no. 1. Elsevier B.V., pp. 48–70, Jan-2019.

641 17. A. Marucci and A. Cappuccini, “Dynamic photovoltaic greenhouse: Energy
642 efficiency in clear sky conditions,” Appl. Energy, vol. 170, pp. 362–376, May 2016.

643 18. M. Cossu, A. Yano, Z. Li, M. Onoe, H. Nakamura, T. Matsumoto, and J. Nakata,
644 “Advances on the semi-transparent modules based on micro solar cells: First
645 integration in a greenhouse system,” Appl. Energy, vol. 162, pp. 1042–1051, Jan.
646 2016.

647 19. G. E. Hassan, A. H. Salah, H. Fath, M. Elhelw, A. Hassan, and K. M. Saqr,
648 “Optimum operational performance of a new stand-alone agricultural greenhouse
649 with integrated-TPV solar panels,” Sol. Energy, vol. 136, pp. 303–316, 2016.

650 20. A. Yano, M. Onoe, and J. Nakata, “Prototype semi-transparent photovoltaic
651 modules for greenhouse roof applications,” Biosyst. Eng., vol. 122, pp. 62–73, 2014.
652 21. T. Yohannes and H. Fath, “Novel Agriculture Greenhouse That Grows Its Water
653 And Power : Thermal Analysis,” Cancam, 2013.
654 22. H. E. S. Fath and K. Abdelrahman, “Micro-climatic environmental conditions
655 inside a greenhouse with a built-in solar distillation system,” vol. 171, pp. 267–287,
656 2004.
657 23. A. A. M. Radhwan, “Transient performance of a stepped solar still with built-in
658 latent heat thermal energy storage,” Desalination, vol. 171, no. 1, pp. 61–76, 2005.
659 24. M. T. Chaibi, “Validation of a simulation model for water desalination in a
660 greenhouse roof through laboratory experiments and conceptual parameter
661 discussions,” Desalination, vol. 142, no. 1, pp. 65–78, Jan. 2002.
662 25. E. G. Mari, R. P. G. Colomer, and C. A. Blaise-Ombrecht, “Performance analysis
663 of a solar still integrated in a greenhouse,” Desalination, vol. 203, no. 1–3, pp. 435–
664 443, 2007.
665 26. A. Radhwan and H. E. S. Fath, “Thermal Performance of Greenhouse with Built-in
666 Solar Distillation System: Experimental Study,” Ninth Int. Water Technol. Conf.,

667 pp. 793–809, 2005.

668 27. A. H. Salah, G. E. Hassan, H. Fath, M. Elhelw, and S. Elsherbiny, “Analytical
669 investigation of different operational scenarios of a novel greenhouse combined
670 with solar stills,” Appl. Therm. Eng., vol. 122, pp. 297–310, 2017.

671 28. O. O. Rabhy, I. G. Adam, M. Elsayed Youssef, A. B. Rashad, and G. E. Hassan,
672 “Numerical and experimental analyses of a transparent solar distiller for an
673 agricultural greenhouse,” Appl. Energy, vol. 253, no. July, p. 113564, 2019.

674 29. H. J. J. Janssen, T. H. Gieling, S. L. Speetjens, J. D. Stigter, and G. Van Straten,
675 “Watergy: Infrastructure for process control in a closed greenhouse in semi-arid
676 regions,” Acta Hortic., vol. 691, no. May 2014, pp. 821–828, 2005.

677 30. H. F. De Zwart, “The sunergy greenhouse - One year of measurements in a next
678 generation greenhouse,” in Acta Horticulturae, 2011, vol. 893, pp. 351–358.

679 31. A. M. Al-Ismaili and H. Jayasuriya, “Seawater greenhouse in Oman: A sustainable
680 technique for freshwater conservation and production,” Renewable and Sustainable
681 Energy Reviews, vol. 54. Elsevier Ltd, pp. 653–664, Feb-2016.

682 32. E. Farrell, M. I. Hassan, R. A. Tufa, A. Tuomiranta, A. H. Avci, A. Politano, E.
683 Curcio, and H. A. Arafat, “Reverse electrodialysis powered greenhouse concept for

684 water- and energy-self-sufficient agriculture," Appl. Energy, vol. 187, pp. 390–409,
685 2017.
686 33. C. B. Maia, F. V. M. Silva, V. L. C. Oliveira, and L. L. Kazmerski, "An overview
687 of the use of solar chimneys for desalination," Sol. Energy, vol. 183, pp. 83–95,
688 2019.
689 34. P. Amarananwatana and C. Sorapipatana, "An Assessment of the ASHRAE Clear
690 Sky Model for Irradiance Prediction in Thailand Nuntiya," Asian J. Energy Environ,
691 vol. 08, no. 02, pp. 523–532, 2007.
692 35. S. Rabia, 2017 ASHRAE Handbook Fundamentals SI.pdf. .
693 36. Abdullahi, K., Salah, A.H., Fath, H.E.S., 2019. Transient operational performance
694 of integrated solar greenhouse – Desalination system: Case study of Mediterranean
695 mild winter condition. p. 030006. https://doi.org/10.1063/1.5117037
696 37. D. Piscia, J. I. Montero, E. Baeza, and B. J. Bailey, "A CFD greenhouse night-time
697 condensation model," Biosyst. Eng., vol. 111, no. 2, pp. 141–154, 2012.
698 38. I. Janajreh, H. E. S. Fath, and S. S. Raza, "Thermal performance of solar-distillation
699 integrated greenhouses," 2012.
700 39. D. Piscia, P. Muñoz, C. Panadès, and J. I. Montero, "A method of coupling CFD

701 and energy balance simulations to study humidity control in unheated greenhouses,"
702 Comput. Electron. Agric., vol. 115, pp. 129–141, 2015.
703 40. T. Boulard and S. Wang, "Greenhouse crop transpiration simulation from external
704 climate conditions," vol. 100, pp. 25–34, 2000.
705 41. J. Chen, F. Xu, D. Tan, Z. Shen, L. Zhang, and Q. Ai, "A control method for
706 agricultural greenhouses heating based on computational fluid dynamics and energy
707 prediction model," Appl. Energy, vol. 141, no. 1, pp. 106–118, 2015.
708 42. "ANSYS Fluent Theory Guide, 2017.
709 43. C. Baxevanou, D. Fidaros, T. Bartzanas, and C. Kittas, "Yearly numerical
710 evaluation of greenhouse cover materials," Comput. Electron. Agric., vol. 149, no.
711 August 2016, pp. 54–70, 2018.
712 44. X. He, J. Wang, S. Guo, J. Zhang, B. Wei, J. Sun, and S. Shu, "Ventilation
713 optimization of solar greenhouse with removable back walls based on CFD,"
714 Comput. Electron. Agric., no. October, pp. 0–1, 2017.
715 45. A. Marucci, D. Monarca, M. Cecchini, A. Colantoni, A. Manzo, and A. Cappuccini,
716 "Films for Mediterranean Greenhouse : A New Sustainable Technology," vol. 2012,
717 2012.

718 46. W. Baudoin, R. Nono-Womdim, “Good agricultural practices for greenhouse
719 vegetable crops: Principles for mediterranean climate areas,” agris.fao.org.
720 47. A. H. Salah and G. E. Hassan, “Performance Improvement of Roof Transparent
721 Solar Still Coupled With Agriculture Greenhouse,” Int. Conf. New Trends Sustain.
722 Energy-ICNTSE, vol. 3, no. 1, pp. 151–154, 2016.
723 48. N. Katsoulas, A. Sapounas, F. De Zwart, J. A. Dieleman, and C. Stanghellini,
724 “Reducing ventilation requirements in semi-closed greenhouses increases water use
725 efficiency,” Agric. Water Manag., vol. 156, pp. 90–99, 2015.
726 49. C. R. Chu, T. W. Lan, R. K. Tasi, T. R. Wu, and C. K. Yang, “Wind-driven natural
727 ventilation of greenhouses with vegetation,” Biosyst. Eng., vol. 164, pp. 221–234,
728 2017.
729

730 **Nomenclature**

Nomenclature

A	apparent solar irradiation	a	mean height of plants
B_c	breadth of channel, m	C	diffuse radiation factor
C_2	inertial resistance	COP	Coefficient of Performance
C_p	specific heat, J/kg K	D_{H2O}	vapor-air diffusion
e	Total fluid energy	H_S	height of south wall, m
H_N	height of north wall, m	h_{fg}	heat of vaporization of water, J/kg
h_j	Sensible enthalpy	h_w	height of water in the TSD, m
h_{out}	enthalpy of outlet air, J/kg	h_{in}	enthalpy of inlet air, J/kg
$I_{B\beta}$	direct beam solar radiation, W/m^2	I_β	incident global solar radiation, W/m^2
$I_{D\beta}$	diffused solar radiation, W/m^2	$I_{R\beta}$	reflected radiation W/m^2
K	thermal conductivity	k	atmospheric extinction coefficient
L_b	Length of TSD base, m	LAI	leaf area index
L	length of the greenhouse, m	k_p	plant leaf Characteristic length, m
M	Mass, kg	m_a	mass flow rate of air, kg/s
m_c	mass flow rate of water, kg/s	m_{cond}	mass flow rate of air through the condenser, kg/s
Pr_t	Prandtl number	Q_e	Evaporated heat, W
Q_{in}	inlet heat to any component	Q_{out}	outlet heat from any component
r_a	plant aerodynamic resistance, s/m	r_s	plant stomata resistance, s/m
S	Source term	Sc_t	Schmidt number
S_h	horizontal space between TSDs, m	S_r	vertical space between TSDs, m

S_i	Momentum sink	T	Temperature
th_g	thickness of glass, m	u_i	Air velocity
$\vec{V}$	Velocity vector	W	Width of greenhouse
w	Absolute humidity, kg(water)/kg(air)	x_i	Cartesian coordinate
α	Absorptivity	Y_{H2O}	Specie concentration
β	GH roof tilted angle	ε	Emissivity
ρ	Density, kg/m^3	∇	Divergence operator
Γ	Diffusion coefficient	τ	Transmissivity
ψ	Latitude angle	μ_t	Turbulent viscosity
p	Plant	ϕ	Concentration variable
ω	Azimuthal angle	gr	Ground
θ_z	Zenith angle on an inclined surface	a_i	Circulating air in the GH cavity
a_2	Exit of condenser	δ	Declination angle

Table 1. Greenhouse geometrical dimensions.

L	8 (m)	β_{TSD}	30°
W	1 (m)	L_b	0.75 (m)
H_S	2.5 (m)	h_w	1 (cm)
H_N	4.5 (m)	S_h	0.5 (m)
B_c	1.5 (m)	S_r	0.75 (m)
th_g	3 (mm)		

736 **Table 2.** CFD parameters used.

CLASSIFICATION	**METHOD**	**Under relaxation factor**	**Parameter**
Solver settings	Pressure-based solver	Pressure	0.3
Pressure-Velocity Coupling	SIMPLE	Density	1
Energy discrete scheme	Second order upwind	Mass Force	0.9
Momentum discrete scheme	Second order upwind	Momentum	0.7
k discrete scheme	First order upwind	H_20	1
e discrete scheme	First order upwind	Energy	1
H_2O scheme	Second order upwind	Turbulent Viscosity	1
		k and e	0.8

737

738 **Table 3**. Plant parameters.

a	1 (m)	LAI	3
$C_{p,\,p}$	2130 (J/kg. k)	α_p	0.4
ε_p	0.92	ρ_p	700 (kg/m^3)
k_p	0.173 (W/m.K)	L_p	0.03 (m)
r_a	50(day) to 5000(night) (S/m)	r_s	250 (S/m)

739
740
741
742
743
744

745 **Table 4**. Thermo-physical material parameters.

Glass		**Water**		**GROUND**	
ε_g	0.92	ε_w	0.4733	ε_{gr}	0.93
α_g	0.06	α_w	0.3	α_{gr}	0.4
τ_g	0.9	τ_w	0.68	τ_{gr}	1 ($W/m^2.K$)
ρ_g	2500 (kg/m^3)	ρ_w	1(Ton/m^3)	ρ_{gr}	1680 (kg/m^3)
$C_{p,g}$	750 (J/kg. k)	$C_{p,w}$	4186 (J/kg.k)	$C_{p,gr}$	1187.8 (J/kg. k)
K_g	1.2 (W/m. K)			K_{gr}	2.15 (W/m. K)

746
747
748
749
750
751
752
753
754
755
756
757
758
759
760
761
762
763

764 **Table 5**. Material's thermal and optical properties.

Material	**Glass**	**P.E**	**EVA**	**PVC film**
Density ρ[kg m^{-3}]	2500	923	926	900
Specific heat C_p[J kg^{-1} K^{-1}]	750	2300	2600	2550
Emissivity	0.92	0.7	0.89	0.91
Absorptivity	0.06	0.1	0.02	0.1
Transmissivity	0.9	0.85	0.89	0.8

765

766

Figures

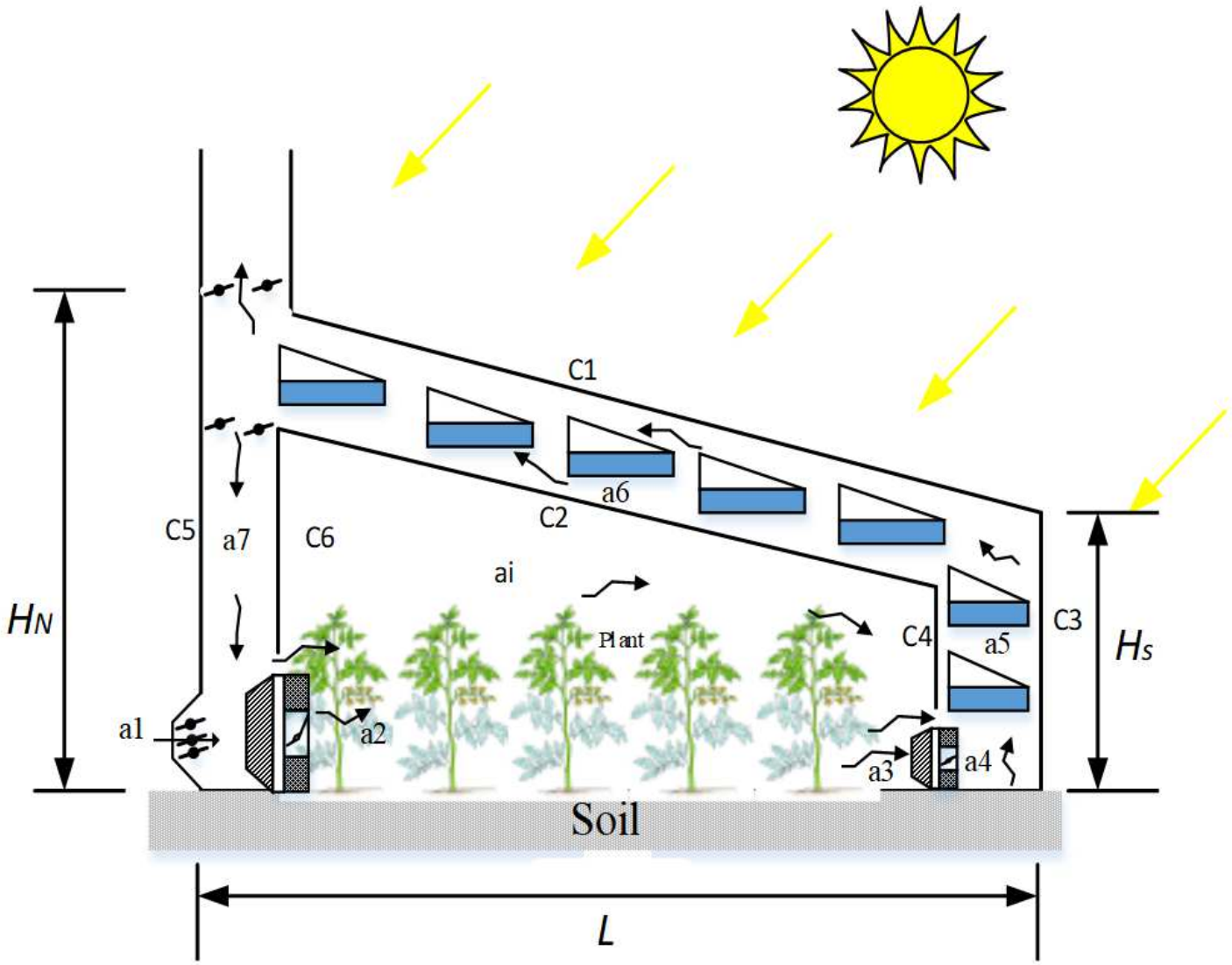

Figure 1

Conceptual configuration of the developed greenhouse.

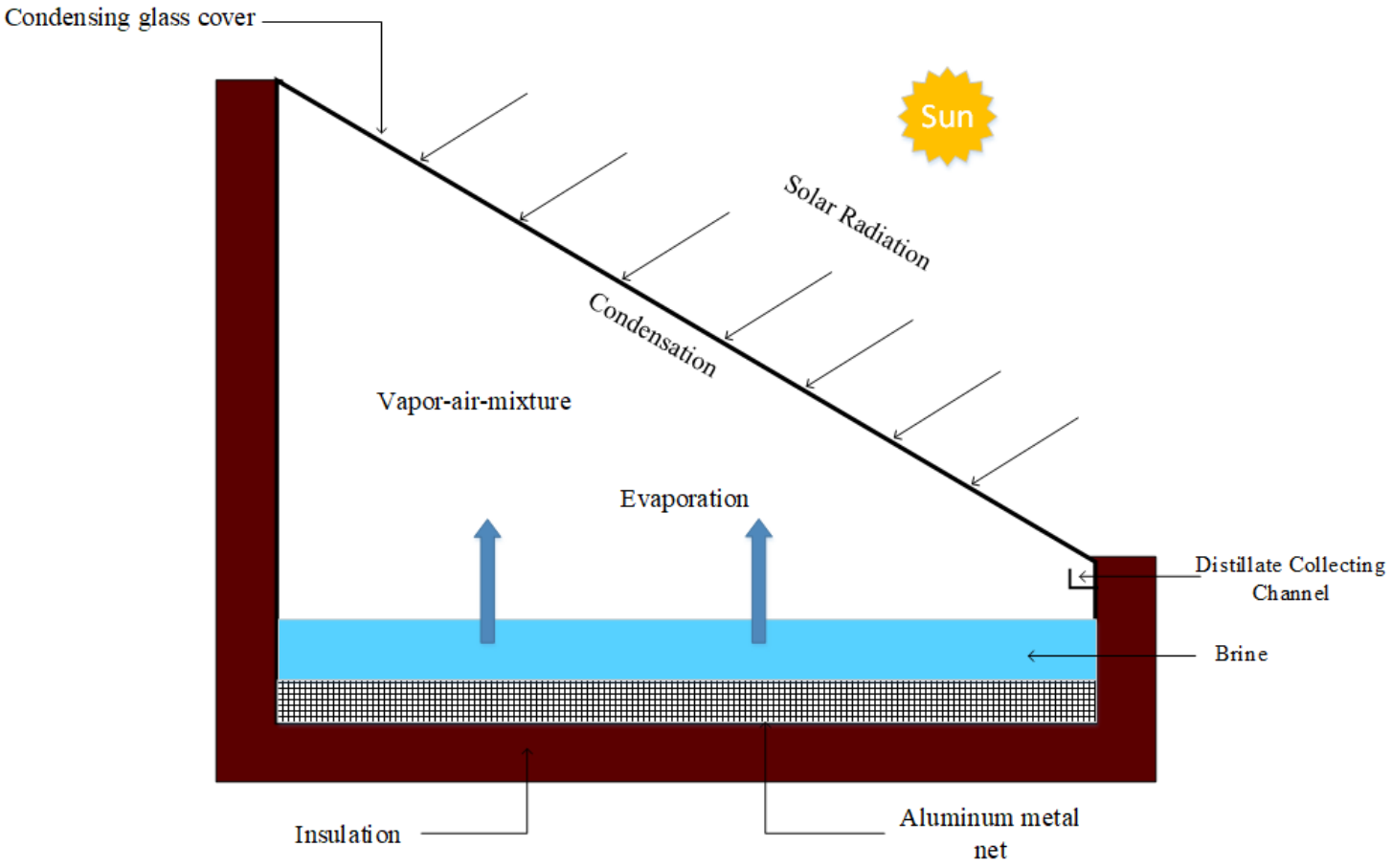

Figure 2

Simple configuration of the transparent solar distillers integrated into the greenhouse roof.

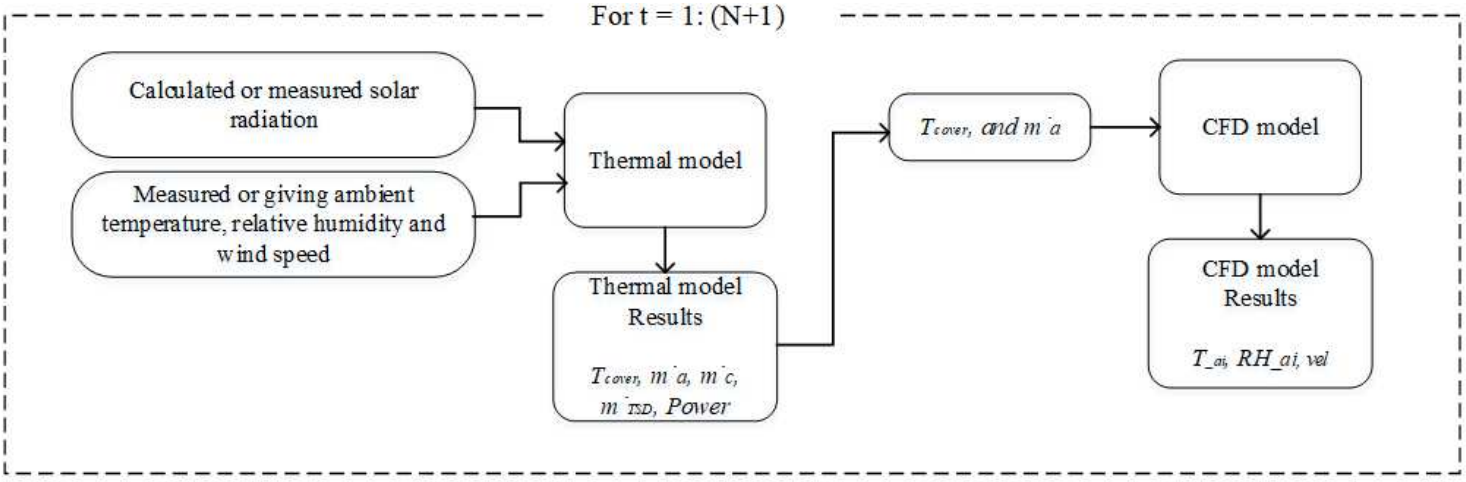

Figure 3

Brief description of the system methodology.

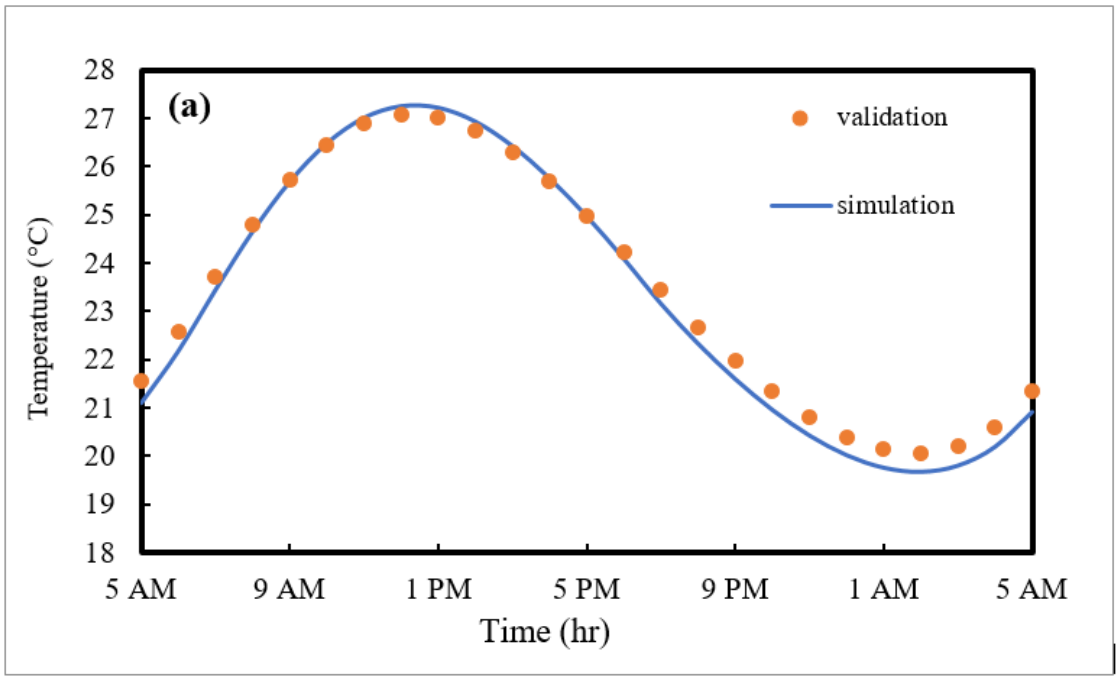

(a) Temperature

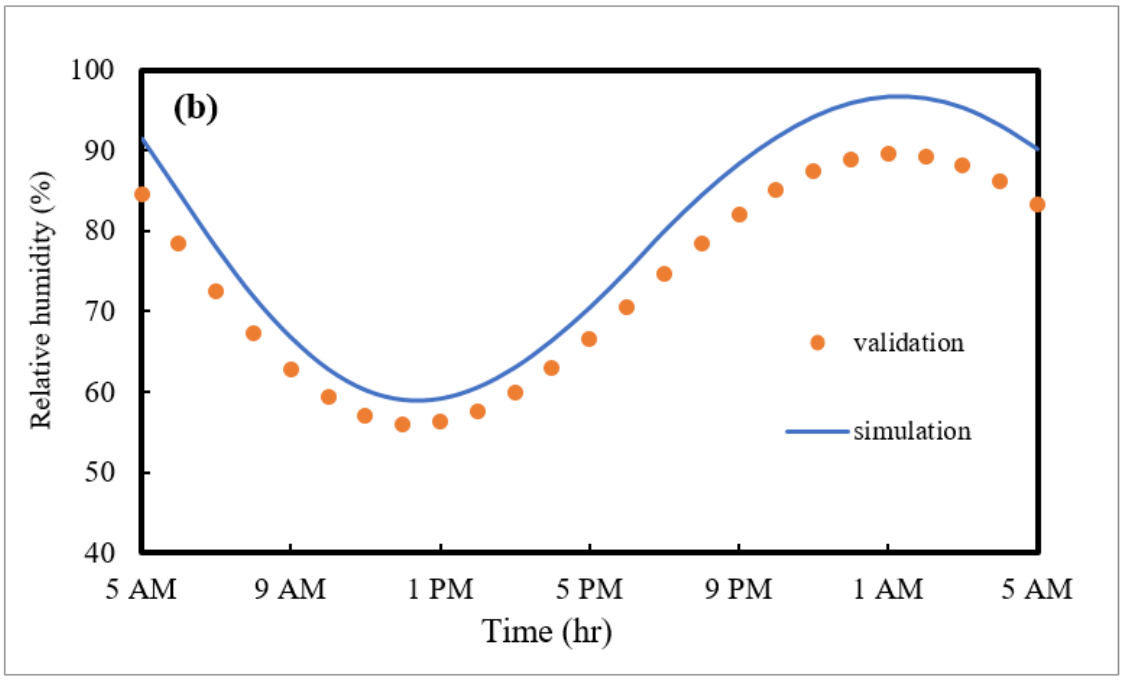

(b) Relative humidity

Figure 4

CFD numerical and validation results of the greenhouse air temperature (a) and relative humidity (b) for a typical day of June.

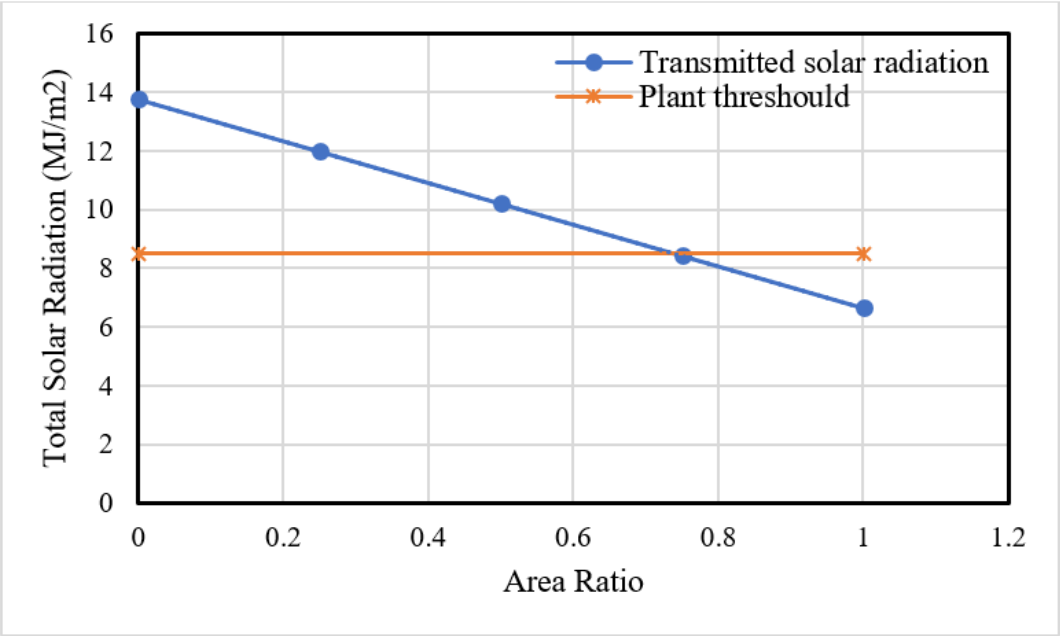

(a) Effect of Al-metal net area ratio on the total solar radiation transmitted into the GH cavity.

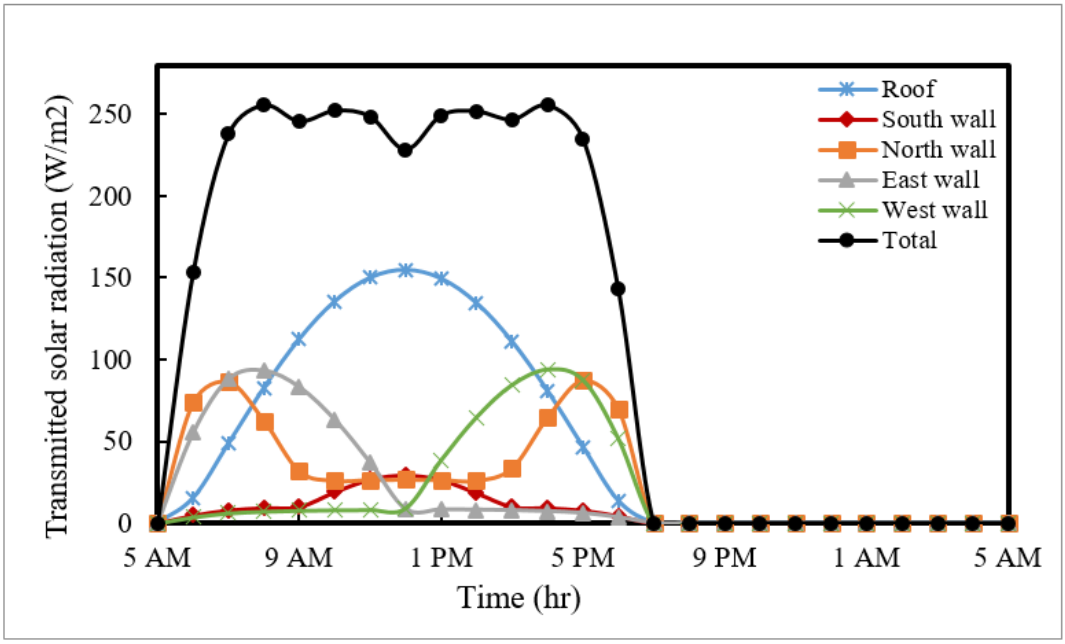

(b) Instantaneous solar radiation transmitted through the roof and walls of the GH

Figure 5

Effect of Al-metal net area ratio and instantaneous solar radiation transmitted into the greenhouse for a typical day of 21st June.

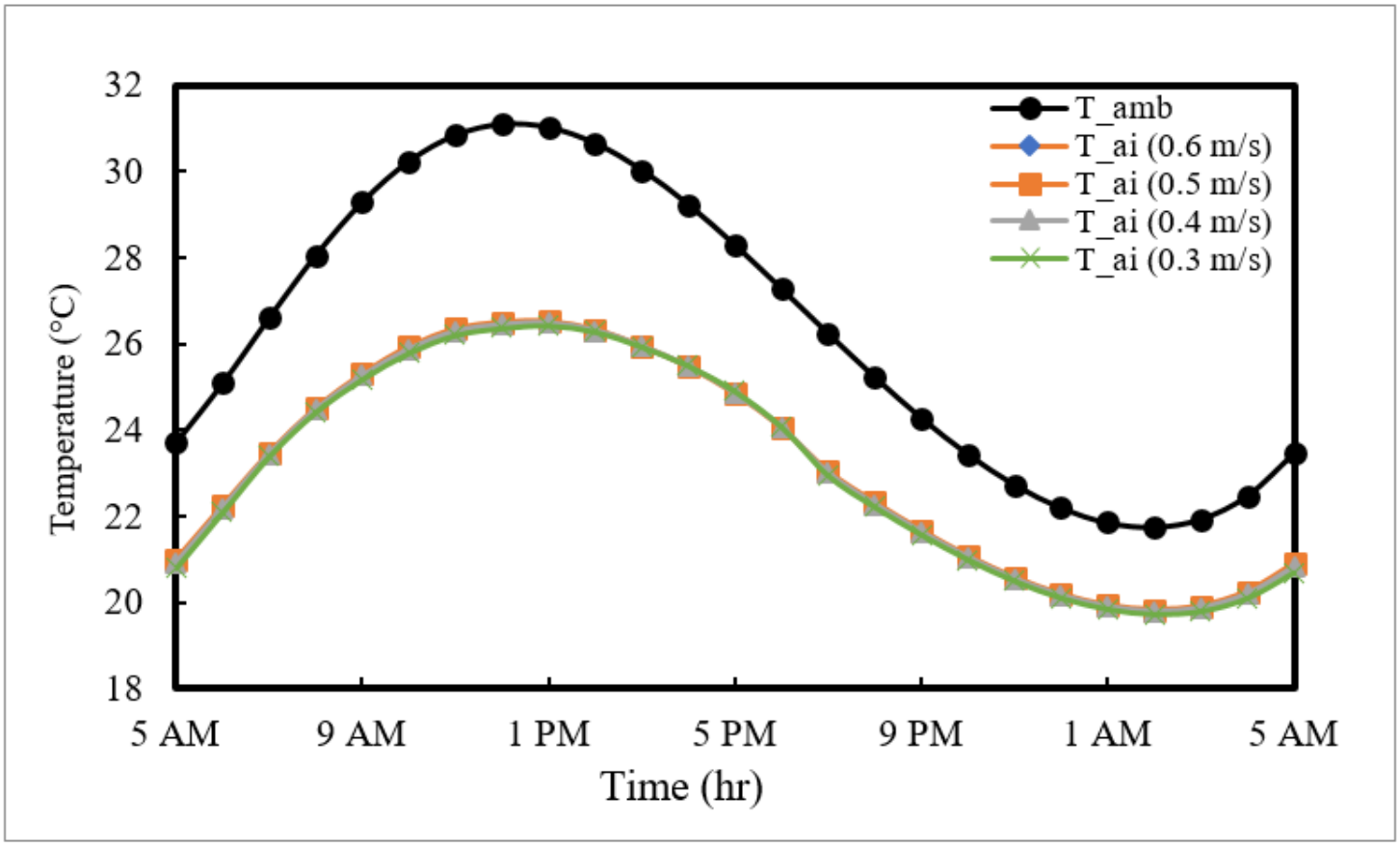

Figure 6

Instantaneously air temperature inside the greenhouse cavity at different air velocity for a typical day of 21st June in Borg AL-Arab Egypt.

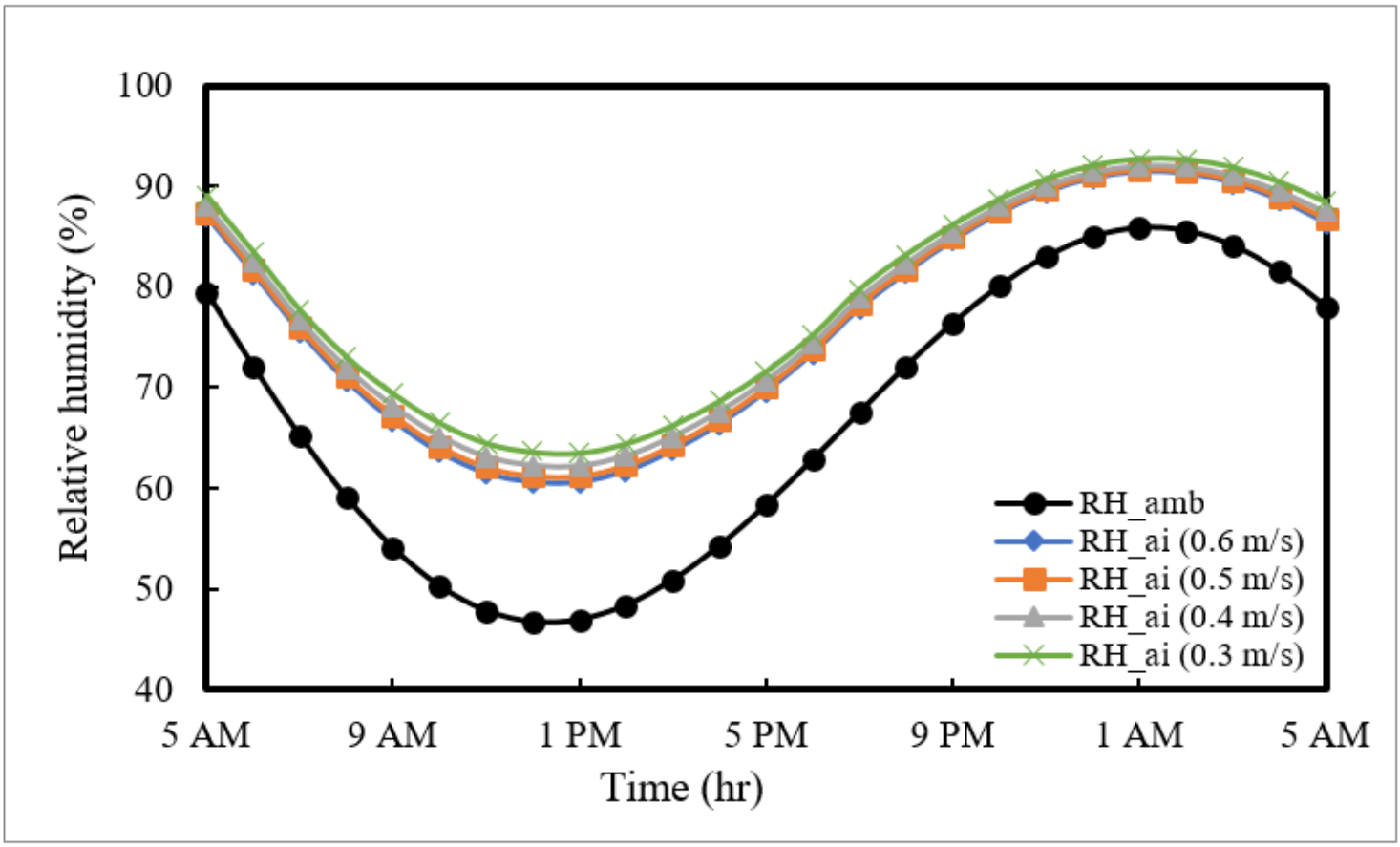

Figure 7

Instantaneously air relative humidity inside the greenhouse cavity at different air velocity for a typical day of 21st June in Borg AL-Arab Egypt.

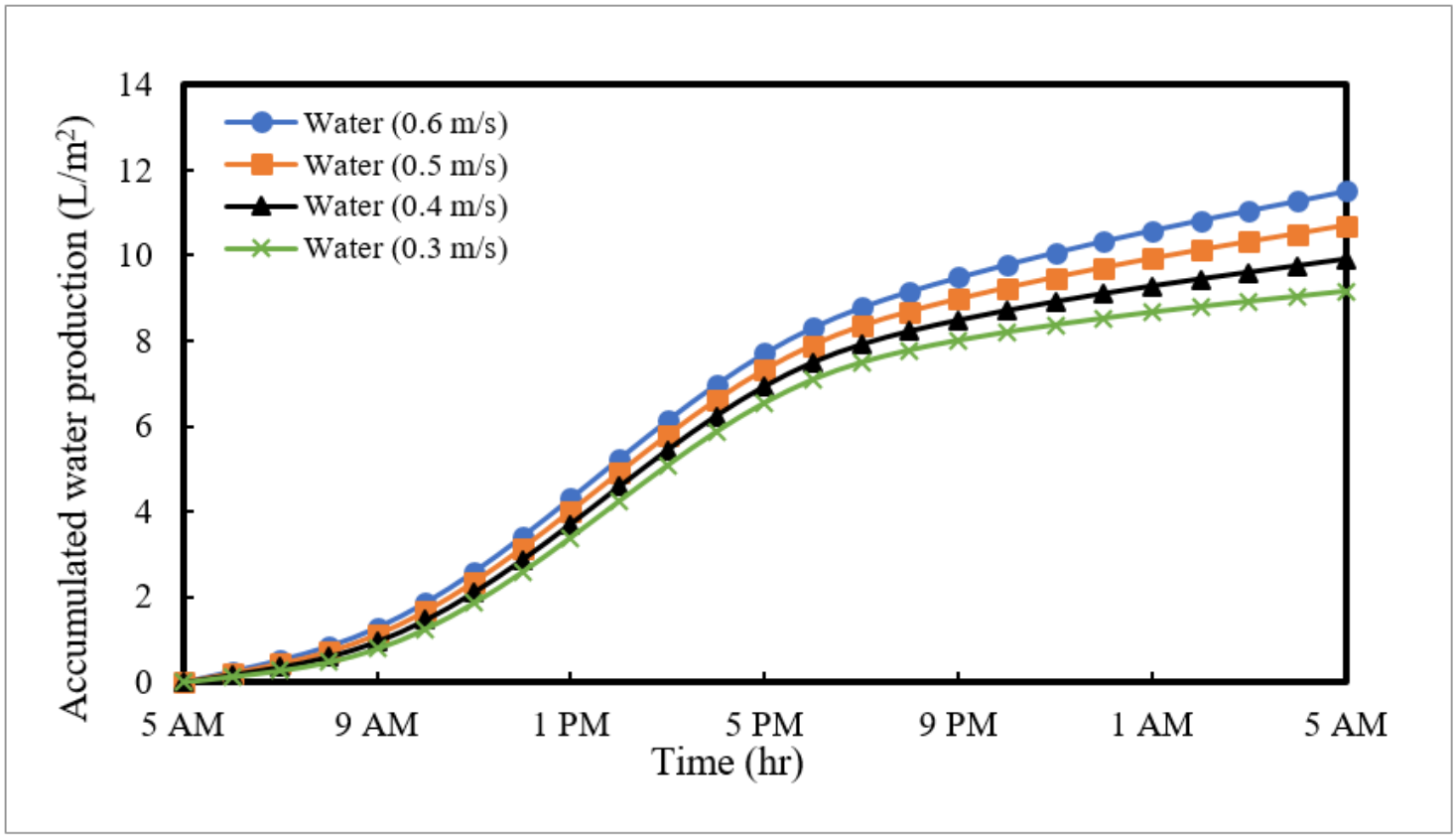

Figure 8

Accumulated water production at different air flow velocities for a typical day of 21st June in Borg AL-Arab Egypt.

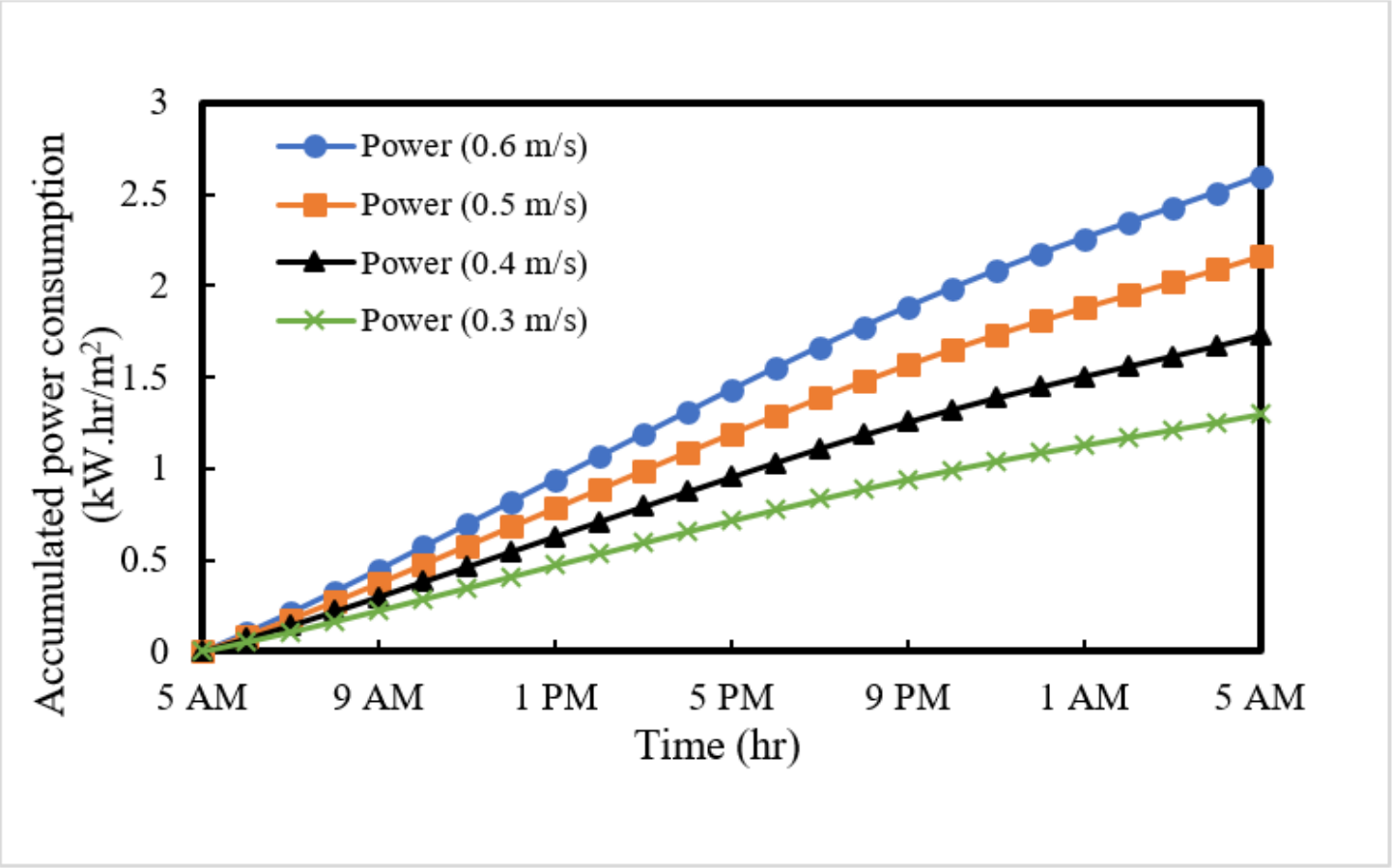

Figure 9

Accumulated power consumption at different air flow velocities for a typical day of 21st June in Borg AL-Arab Egypt.

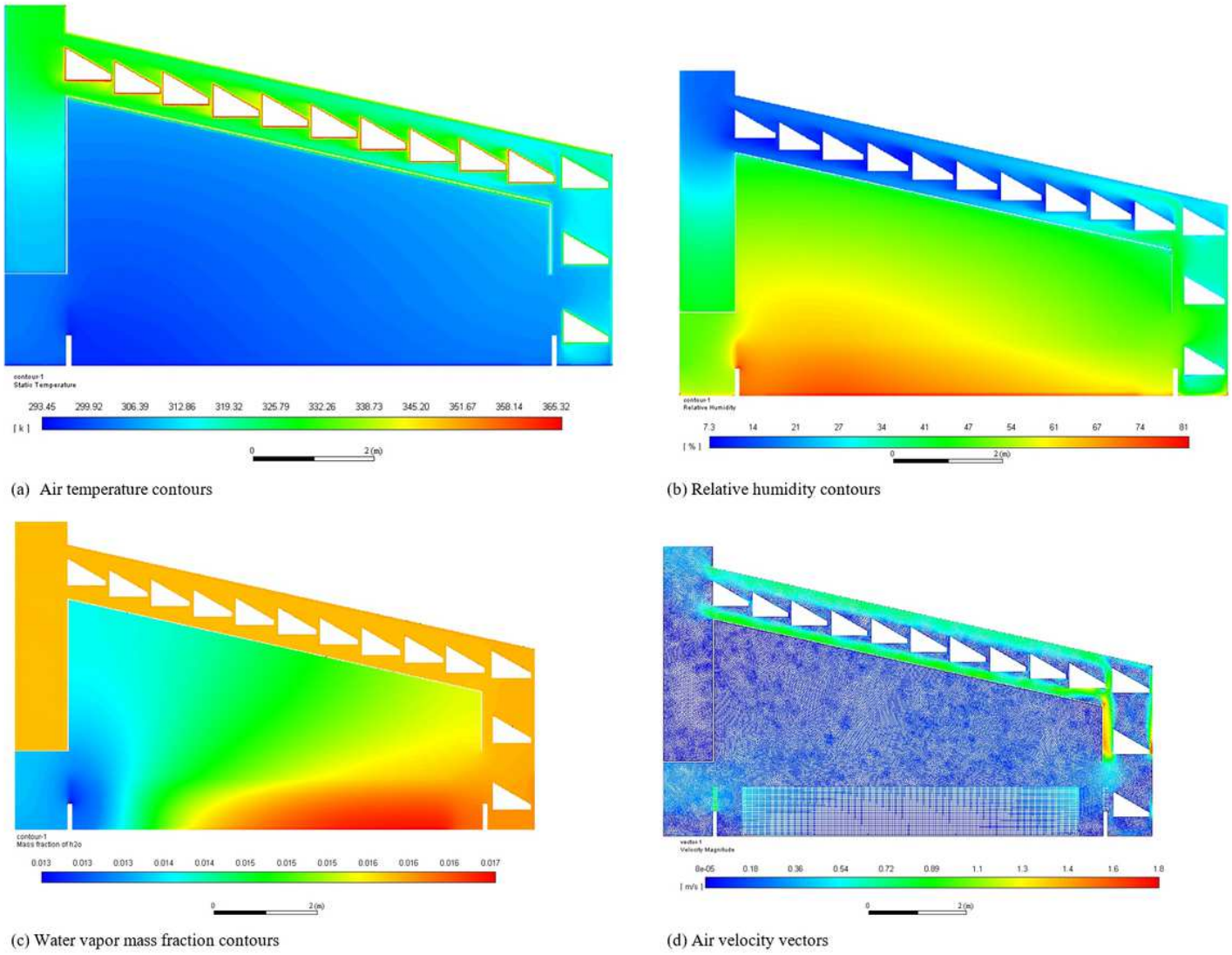

Figure 10

CFD simulation results for air temperature, relative humidity, vapor mass fraction and velocity vector contours inside the GH at midday of the 21st of June in Borg AL-Arab Egypt.

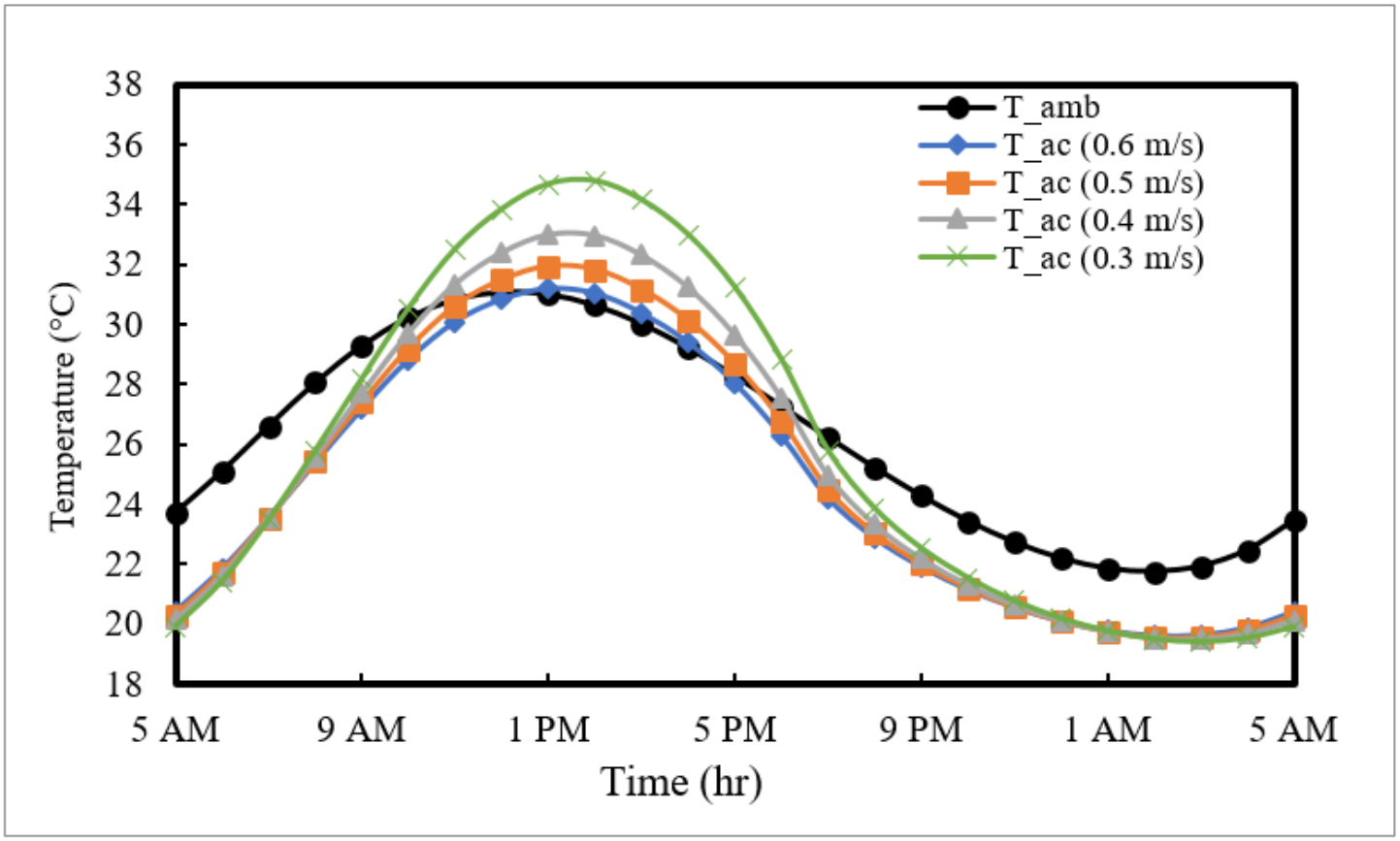

Figure 11

Air Temperature at inclined riser for different air flow velocity for a typical day of 21st June in Borg AL-Arab Egypt.

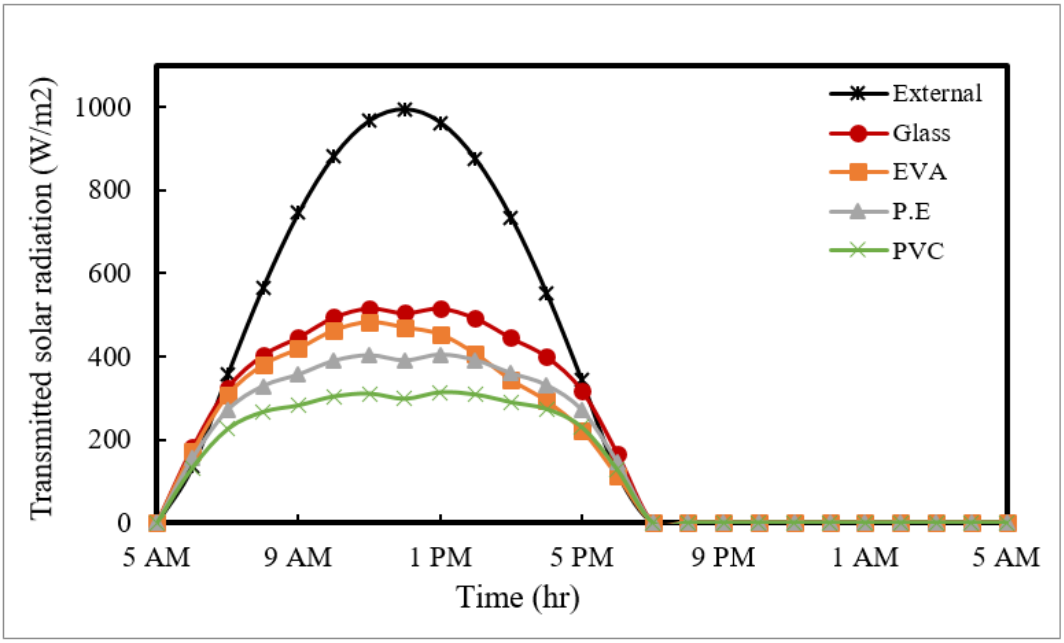

(a) Instantaneously total solar radiation transmitted into GH cavity for different covering materials

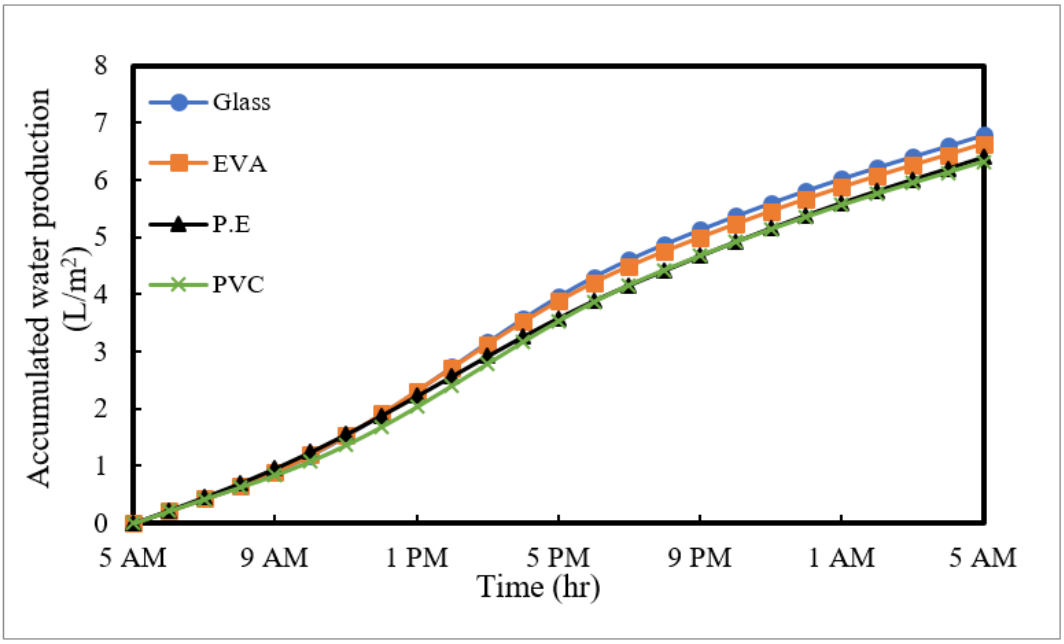

(b) Accumulated water production for different covering materials

Figure 12

Transmitted solar radiation and water production for different covering materials on the 21st of June in Borg Al-Arab Egypt.

Supplementary Files

This is a list of supplementary files associated with this preprint. Click to download.

- Supplementary.docx